ACS SENSORS

Article

Cite This: ACS Sens. 2020, 5, 242−249

pubs.acs.org/acssensors

Bioimaging of Glutathione with a Two-Photon Fluorescent Probe and Its Potential Application for Surgery Guide in Laryngeal Cancer

Yuxia Zou,[†,‡,§] Mingshun Li,[†,§] Yanlong Xing,[*,†] Tingting Duan,[‡] Xuejun Zhou,[*,†,‡] and Fabiao Yu[*,†,‡]

[†]Institute of Functional Materials and Molecular Imaging, Key Laboratory of Emergency and Trauma, Ministry of Education, Key Laboratory of Hainan Trauma and Disaster Rescue, College of Clinical Medicine, College of Emergency and Trauma, Hainan Medical University, Haikou 571199, China

[‡]Department of Otolaryngology, Head and Neck Surgery, The First Affiliated Hospital of Hainan Medical University, Haikou 570102, China

Supporting Information

ABSTRACT: As the most abundant nonprotein biothiol in living cells, glutathione (GSH) prevents cellular components from oxidative damage and maintains the intracellular redox homeostasis. For further exploring whether GSH can be employed as a bioindicator to discriminate tumor lesion at a cellular level, the highly selective detection and accurate quantification of GSH under pathological conditions are critical. Herein, we design a coumarin derivative-based two-photon fluorescent probe **Cou-Br** for the detection of GSH in living cells, mice models, and clinical specimens. The prepared probe is capable of sensitively and selectively detecting GSH in complex biological systems. **Cou-Br** displays a good linear relationship in response to GSH and a low limit of detection. With the fluorescence signal positively associated with intracellular GSH levels, the probe enables real-time imaging of GSH in various cell lines. Under the condition of CS_2 stimulation, **Cou-Br** can rapidly respond to the fluctuation of intracellular GSH induced by oxidative damage. Furthermore, the in situ and in vivo bioimaging performances of **Cou-Br** are demonstrated. Typically, relying on the different cellular concentrations of GSH, the probe is successfully employed to identify the human laryngeal cancer lesion with outstanding capabilities of deep tissue imaging and tumor margin recognition. We assume that the abnormal expression level of GSH may be utilized as a potential bioindicator to discriminate tumor tissues from the surrounding disease-free tissues. To conclude, the proposed probe **Cou-Br** may potentially serve as a powerful chemical tool for the surgical navigation of cancer in clinic.

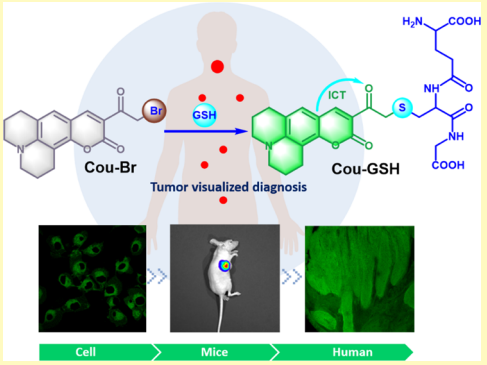

KEYWORDS: *fluorescent probes, two-photon, glutathione, cell imaging, in vivo imaging, laryngeal cancer*

Glutathione (GSH) is widely present in living cells with antioxidation effects and composed of glutamic acid, cysteine, and glycine.[1,2] It plays vital roles in the biochemical defense system and has a string of physiological functions. As an important antioxidant species in vivo, it can protect the sulfhydryl groups in proteins and enzymes and thus maintain their redox state.[3−5] The concentrations of intracellular GSH is ∼0.5−15 mM depending on different types of cells.[6] As reported, the levels of GSH varies remarkably between healthy and cancer tissues. For instance, plenty of clinical studies have demonstrated that significant increase in GSH levels is detected in laryngeal cancer tumors, compared to either normal controls or peritumoral tissues.[7] Laryngeal cancer is a common malignant tumor of the head and neck and had induced over 1% death worldwide in 2018.[8] In spite of the improved therapy methods of laryngeal cancer, the 5 year survival rate of patients has not been obviously ameliorated in the past decades. Therefore, the effective control and cure of laryngeal cancer remains a strict challenge in clinical practice.

Currently, surgery is still the "Gold-standard" therapy of solid tumors.[9] However, the presence of remaining tumor cells, that is the positive margin of surgical specimens, is associated with increased local recurrence and poor prognosis for cancer.[10] There is no doubt that the complete resection of laryngeal cancer tissue can improve patient survival and cure rate. The current surgical margin determination mainly relies on intraoperative real-time frozen slices, which is inconvenient and has limited accuracy.[11] Although imaging technologies such as computed tomography (CT) and magnetic resonance imaging (MRI) have been used for real-time determination of the tumor boundaries and provide macroscopic imaging of the tissue, these techniques still suffer from the ambiguous judgment on the surgical margin at the cellular level and the finite application during surgery.[12−14] Bioimaging with small-molecule fluorescent probes has been applied for surgical navigation in animal models[15,16] due to their high sensitivity, noninvasive analysis, and real-time detection.[17−22] Owing to the high expression level of GSH in laryngeal cancer, we

Received: October 29, 2019
Accepted: December 9, 2019
Published: December 9, 2019

DOI: 10.1021/acssensors.9b02118
ACS Sens. 2020, 5, 242−249

hypothesize that the abnormal concentration of GSH may be employed as a bioindicator for identifying the solid tumor, so as to accurately distinguish cancer tissues from the surrounding normal tissues at the cellular level using small-molecule fluorescent probes and thus to improve the treatment of laryngeal cancer. Up to date, several fluorescent probes for the detection of intracellular GSH have been elegantly demonstrated;[23−26] however, the application in clinical specimens is still rarely reported so far to the best of our knowledge. Therefore, it is urgently desired to develop a fluorescent probe with outstanding performances in sensing GSH both in vitro and in vivo.

Recent studies on small molecular fluorescent probes have proven that the two-photon fluorescence imaging possesses the advantages of slight light damage, subtle bleaching area, high spatial and temporal resolutions, and deep tissue penetration.[27−30] Thus, it is considered that the two-photon fluorescent probes can be ideal chemical tools for intraoperative imaging.

Herein, we designed and synthesized a two-photon fluorescent probe **Cou-Br** for imaging of GSH in living cells, mice models, and human clinical cancer tissues with the aim to verify the indicative and predictive roles of GSH in locating laryngeal tumor. **Cou-Br** was composed of a coumarin derivative based fluorophore and a brominated recognition unit, which responded to GSH with a "turn-on" fluorescence switch. The probe exhibited a good linear relationship for GSH in the concentration range of 0−15 mM, as well as satisfying the sensitivity and selectivity for GSH detection in complicated biological systems. Moreover, the probe could rapidly respond to the fluctuation of the intracellular GSH concentration stimulated by exogenous carbon disulfide (CS_2). Finally, **Cou-Br** was successfully applied to discriminate the boundary of the laryngeal cancer tissues from normal tissues in both mice models and actual human clinical specimens. The results evidently elucidated the potential utilization of **Cou-Br** to accurately discriminate tumor tissues based on the differentiated imaging output of GSH in laryngeal cancer tumors and peritumoral tissues.

EXPERIMENTAL SECTION

Synthesis of Probe Cou-Br. All reactions were performed under argon protection in dark environment and monitored by thin-layer chromatography. Flash chromatography was carried out using silica gel (200−300 mesh). The synthetic routes of other compounds can be found in the Supporting Information (Figure S1). A solution of CuBr (0.4467 g, 2 mmol) in ethanol (10 mL) was added dropwise to a solution of compound **2** (0.2833 g, 1 mmol) in ethanol (15 mL) at 75 °C. After overnight reaction, the mixture was cooled to room temperature. The resulting precipitate was filtered and purified by silica gel column chromatography (eluent: 50−100% CH_2Cl_2 in petroleum ether) to afford probe **Cou-Br** (0.1336 g, 37%) as a tawny solid. ^{1}H NMR (400 MHz, DMSO-d_6) δ (ppm): 8.45 (s, 1H), 7.29 (s, 1H), 4.61 (s, 2H), 3.38−3.35 (t, 4H), 2.75−2.67 (m, 4H), 1.90−1.86 (t, 4H). ^{13}C NMR (100 MHz, DMSO-d_6) δ (ppm): 180.02, 177.29, 162.70, 158.96, 154.25, 147.82, 139.37, 128.58, 120.11, 57.91, 50.19, 49.67, 27.22, 20.85, 19.97, 18.01. HR-MS (ESI$^+$): m/z $[C_{17}H_{16}BrNO_3]^+$ calcd 361.0314, found $[M + H]^+$ 362.0389.

Preparation of Orthotopic Mice Models of Laryngeal Cell Carcinoma. BALB/c mice (25−30 g) were provided by Hainan Medical University. The cancer cells were inoculated with conventionally cultured human pharyngeal carcinoma cell line (FaDu). The FaDu cells were harvested in logarithmic growth phase, after being digested with 0.25% trypsin, washed twice with PBS, and centrifuged at 1000 rpm (12 000 rpm 15 mL) for 5 min. Afterward, the cells were suspended in a 0.9 % sodium chloride solution and fixed to a volume of 5×10^6 (0.2 mL/mouse) in the throat of BALB/c nude mice. The nude mice laryngeal tumor models were successfully established after 3 weeks.

Clinical Specimen Experiments. Human laryngeal carcinoma tissues were obtained from the First Affiliated Hospital of Hainan Medical University. Fresh human laryngeal carcinoma tissues were first resected, followed by adding the embedding agent. After rapid freezing, the frozen tissues were used to prepare 5 and 100 μm tissue slices using a Leica CM1520 slicer. The 5 μm slices were immediately fixed with formaldehyde and stained with hematoxylin−eosin (H&E) and the 100 μm slices were immediately incubated with **Cou-Br** for imaging. The Ethics Committee of Hainan Medical University approved this study. All surgical procedures and experimental protocols were approved by the Institutional Animal Care and Use Committee in Hainan Medical University, Haikou, China.

RESULTS AND DISCUSSION

Design and Synthesis of Cou-Br. The chemical structure of **Cou-Br** and the proposed reaction mechanism of **Cou-Br** with GSH are shown in Scheme 1. It is reported that coumarin

Scheme 1. Molecular Structure of Cou-Br and Its Proposed Response Mechanism toward GSH

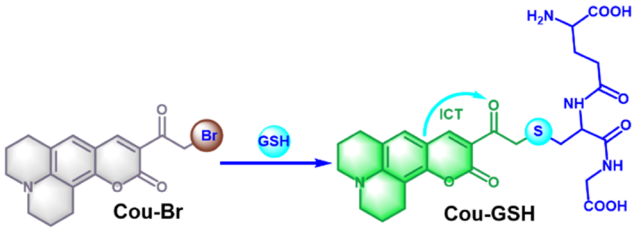

is a class of oral anticoagulant in medicine that possesses high biocompatibility.[31] As a fluorophore, it exhibits excellent two-photon performances including high imaging contrast, good photostability, high quantum yield, and a deeper tissue penetration than one-photon fluorophores. Accordingly, a coumarin derivative was chosen to act as the fluorescence signal transducer.[32] A brominated functional component serves as the fluorescence modulator for recognizing intracellular GSH. The probe is originally nonfluorescent as a result of the heavy-atom effect of bromine atom. In the presence of GSH, the brominated moiety can be substituted by the sulfhydryl group (−SH) in GSH via a strong nucleophilic reactivity, accompanied by the strong fluorescence emission. Other nonprotein biothiols such as cysteine (Cys) and homocysteine (Hcy) share similar reaction mechanisms with GSH because of the sulfhydryl groups in their chemical structures. However, when reacts with the probe **Cou-Br**, 6-membered rings are formed through intramolecular condensation as a result of the appropriate distance between the amino ($-NH_2$) and carbonyl groups (−C═O) in Cys and Hcy (Scheme S1). The formation of the Schiff base intermediate may attenuate the internal charge transfer (ICT) effect in coumarin fluorophore, and the final product provides a faint fluorescence.[23] The concentrations of intracellular GSH is ∼0.5−15 mM, while the levels of Cys and Hcy in the cells are ∼237 and ∼15 μM, respectively.[33] Therefore, neglectable interference may be introduced when detecting GSH in cells (Figure S2a). The design strategy makes the proposed probe **Cou-Br** as a suitable candidate to specifically detect GSH in complex biosystems.

Spectral Properties and Selectivity of Cou-Br. The spectral properties of **Cou-Br** were investigated under

DOI: 10.1021/acssensors.9b02118
ACS Sens. 2020, 5, 242−249

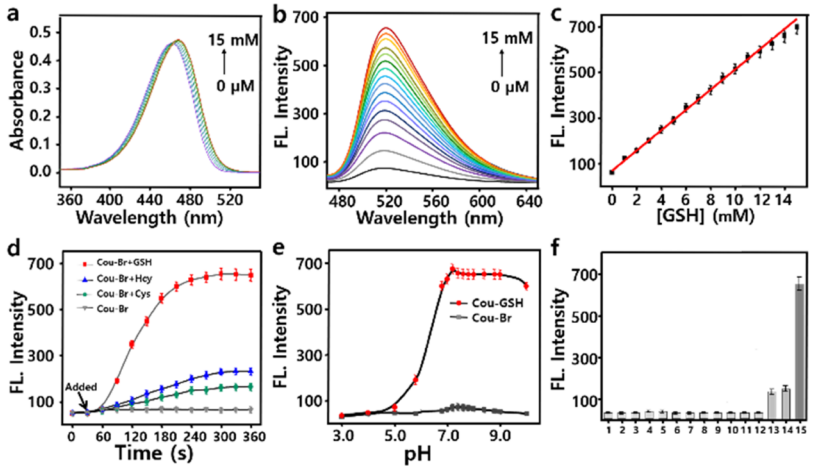

Figure 1. Spectral properties and selectivity of **Cou-Br**. (a) Absorbance spectra of **Cou-Br** (10 μM) toward GSH. Data were recorded after 5 min incubation with increasing concentration of GSH (0−15 mM) in HEPES (pH 7.4, 10 mM). (b) Dose-dependent emission spectra of **Cou-Br** (10 μM) toward GSH. λ_{em} = 520 nm. (c) Linear relationship between fluorescence (FL) intensities at 520 nm and GSH concentrations (0−15 mM). (d) Time-dependent fluorescence intensity of probe **Cou-Br** toward GSH (10 mM), Cys (15 mM) and Hcy (15 mM) during 0−360 s, respectively. (e) Fluorescence signal changes of **Cou-Br** (10 μM) and Cou-GSH (10 μM) at various pH values from 3.0 to 10.0 (10 mM HEPES buffer). (f) Fluorescence intensity (at 520 nm) of **Cou-Br** (10 μM) responding to various analytes in HEPES. 1, Blank; 2, histidine (10 μM); 3, glycine (10 μM); 4, alanine (10 μM); 5, glutamic acid (10 μM); 6, arginine (10 μM); 7, proline (10 μM); 8, methionine (10 μM); 9, tyrosine (10 μM); 10, lysine (10 μM); 11, tryptophan (10 μM); 12, serine (10 μM); 13, Hcy (15 mM); 14, Cys (15 mM); and 15, GSH (10 mM). The experiments were repeated three times, and the data are shown as mean (± s.d.).

physiologically relevant conditions (4-(2-hydroxyethyl)-1-piperazineethanesulfonic acid (HEPES), 10 mM, pH 7.4). Data were recorded after incubation with increasing concentrations of GSH in HEPES (pH 7.4, 10 mM) for 5 min at 37 °C. As shown in Figure 1a, the probe had a strong absorption centered at 462 nm. We next studied the fluorescence response of **Cou-Br** to different concentrations of GSH, which displayed gradually increased emission profiles with increasing concentration of GSH (Figure 1b). In addition, a satisfied linear response was obtained between the fluorescence intensities and GSH in the concentration range from 0 to 15 mM (Figure 1c). The linear fitting equation was $F_{520\ nm}$ = 42.9319 × [GSH] mM + 82.273 with a correlation coefficient (r) of 0.9956. Based on the standard method of $3\sigma/k$, the limit of detection for GSH was estimated to be 79 μM, and the experimental detection limit was determined to be 90 μM. This result indicated that the probe could sensitively detect GSH in vitro. Due to the rapid metabolism and instability of GSH in biological systems, the reaction kinetics of **Cou-Br** toward GSH was assessed in HEPES buffer solution (10 mM, pH 7.4). As illustrated in Figure 1d, the probe displayed a small increment in fluorescence intensity after reaction with Hcy and Cys. In contrast, after the addition of GSH, the fluorescence response rapidly increased and reached a plateau within 5 min. The result proved the possibility of further applying **Cou-Br** to the real-time imaging of GSH in cells. Subsequently, the effects of pH on the probe was checked. As manifested in Figure 1e, the fluorescence intensity of the probe **Cou-Br** itself hardly changed under different pH values. Furthermore, in the presence of GSH, an obviously increase in fluorescence signal was observed and remained relatively stable over the physiological pH range, indicating the high photostability of our probe in a biologically relevant system. Considering the complexity of biological environment, herein, the selectivity of **Cou-Br** for GSH was evaluated. At the high level of 15 mM, Cys and Hcy caused a certain degree of fluorescence changes; however, further coexisting interference experiment at the physiological level at Cys (250 μM) and Hcy (15 μM) resulted in almost no fluorescence response (Figure S2a,c). The interference from other biological species including physiologically related amino acids (Figure 1f), reactive oxygen/nitrogen species (Figure S2c), ions and anions (Figure S2d), and protein thiols (Figure S2e) was also examined. The results demonstrated that the probe could selectively detect GSH without interference from other biologically relevant species. All of the above results clearly indicated the feasibility in using the probe **Cou-Br** to rapidly detect GSH with high sensitivity and selectivity in physiological conditions. The fluorescence quantum yield (Φ_f) of the reaction product Cou-GSH was determined to be 0.375 based on the classical method (S1).[34] The two-photon absorption cross sections of Cou-GSH was evaluated as 51 GM with an excitation wavelength at 900 nm via a reported approach (S1).[35]

Detecting and Imaging of GSH in Various Living Cell Lines. After demonstrating the prominent chemical performance of **Cou-Br**, we next applied this probe to detect and image GSH in living cells. Given that GSH played pivotal roles in keeping the redox homeostasis in organisms, we intended to verify the bioimaging of **Cou-Br** in various tumor cell lines, which were related to different systems of human, including FaDu cell line (head and neck), human nonsmall cell lung cancer cell line (A549, chest), human hepatocellular liver carcinoma cell line (HepG2, abdomen), human ovarian cancer cell line (OVCRA-3, pelvic cavity), and human gastric adenocarcinoma cell line (SGC-7901, gastrointestinal tract). First, the cytotoxicity of **Cou-Br** was measured using a Cell Counting Kit-8 (CCK-8) assay at the increasing concentrations of the probe (0.001, 10, 20, 30, 40, 50, 60, 70, 80, 90, and 100 μM). As illustrated in Figure S3, the probe featured low cytotoxicity and high biocompatibility. Afterward, FaDu cell line was chosen as the testing cell model. These cells were simultaneously incubated with nuclear dye 4′,6-diamidino-2-phenylindole (DAPI) and our probe **Cou-Br**. The fluorescent images clearly displayed that the localization of the probe **Cou-**

DOI: 10.1021/acssensors.9b02118
ACS Sens. 2020, 5, 242−249

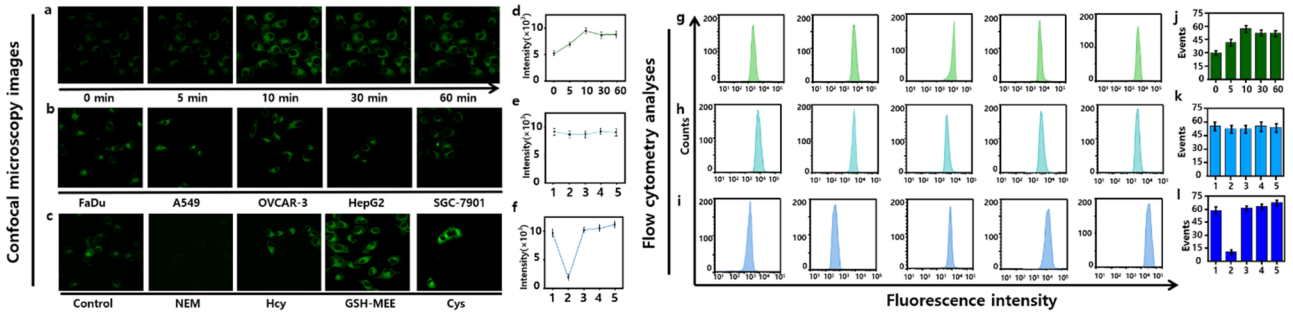

Figure 2. Confocal microscopy images (λ_{ex} = 900 nm, λ_{em} = 500−540 nm) and flow cytometry assays (λ_{ex} = 480 nm, λ_{em} = 500−540 nm) for the detection of GSH in different cell lines. (a) Fluorescent imaging of GSH in FaDu cells at time points: 0, 5, 10, 30, and 60 min. (b) Fluorescent imaging of the GSH in different cells lines: human pharyngeal carcinoma cell line (FaDu cell line), human nonsmall cell lung cancer cell line (A549), human hepatocellular liver carcinoma cell line (HepG2), human ovarian cancer cell line (OVCRA-3), and human gastric adenocarcinoma cell line (SGC-7901). (c) Fluorescent imaging of the GSH in FaDu cells exposed to different stimulation agents: *N*-ethylmaleimide (NEM, 5 mM), Hcy (5 mM), glutathione monoethyl ester (GSH-MEE, 5 mM), and Cys (0.5 mM) were separately added in each group and incubated for 30 min. (d−f) Mean fluorescence intensities of images in (a−c). (g−i) Flow cytometry analyses of images in (a−c). (j−l) Mean values of images in (g−i). The data are shown as mean (± s.d.).

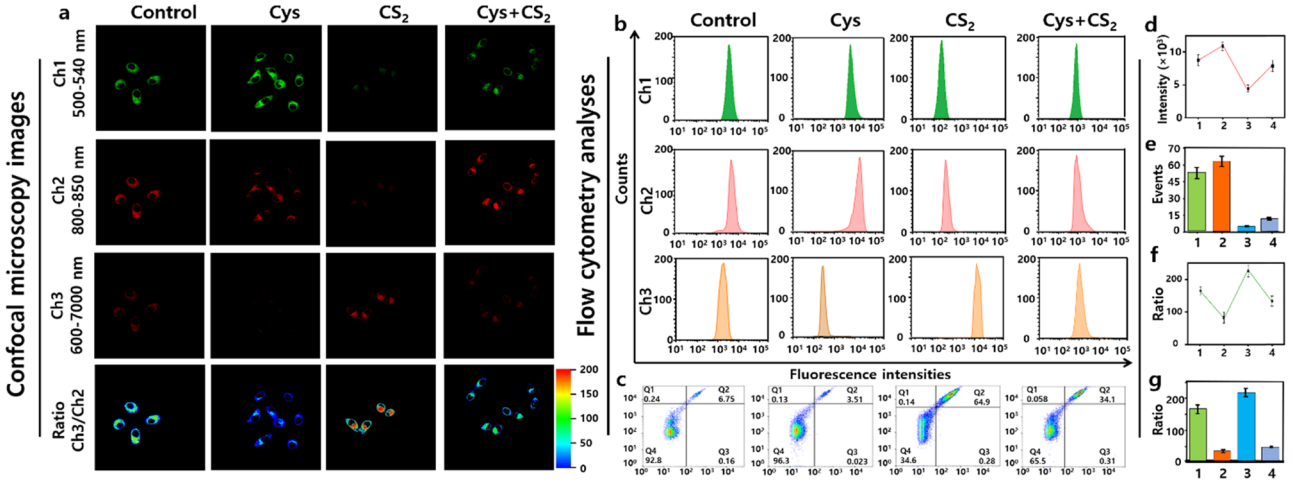

Figure 3. Detection of the GSH fluctuation in living FaDu cells with **Cou-Br**. Fluorescence collection windows: Ch1: λ_{ex} = 900 nm, λ_{em} = 500−540 nm; Ch2: λ_{ex} = 750 nm, λ_{em} = 800−850 nm; and Ch3: λ_{ex} = 545 nm, λ_{em} = 600−700 nm. The FaDu cells were treated with Cys (100 μM, 24 h), CS_2 (5 μM, 6 h) and Cys (100 μM, 24 h), and CS_2 (5 μM, 6 h), respectively. Consequently, **Cou-Br** (10 μM) and **Cy-PFS** (10 μM) were added simultaneously and incubated for 10 min at 37 °C before confocal imaging and flow cytometry analyses. (a) Fluorescent imaging of GSH (channel 1, abbreviated as Ch1, so as the following), H_2O_2 (Ch2, fluorescence collection windows: λ_{ex} = 750 nm, λ_{em} = 800−850 nm) (Ch3: λ_{ex} = 545 nm, λ_{em} = 600−700 nm), and the ratio of Ch3/Ch2. (b) Flow cytometry analyses for the cells in a. (c) Apoptosis detection by flow cytometry analysis. Q1: necrosis cells, Q2: late apoptotic cells, Q3: early apoptotic cells, Q4: survival cells. (d) Mean fluorescence intensities of the images in a (Ch1). (e) Mean values of b (Ch1). (f) Average ratio values in a (Ch3/Ch2). (g) Average ratio values in b (Ch3/Ch2). The data were shown as mean (± s.d.).

Br was in cell cytosol (Figure S4a). The optimal incubation time of **Cou-Br** was also investigated after adding the probe (10 μM) to FaDu cells. As shown in Figure 2a, the probe-incubated cells gradually increased and then maintained fluorescence for 2 h (Figure S4b). Together with the quantitative analysis shown in Figure 2d, these results indicated that the saturated fluorescence occurred after 10 min of incubation, and thus the ideal incubation time was determined at 10 min. Flow cytometry assays (Figure 2g,j) exhibited well-consistent results with the imaging output (Figure 2a). In the next step, the probe **Cou-Br** was applied to various living cell lines for examining its capability of visualization of GSH. As shown in Figure 2b, the probe was well adapted to the biological environment and could image GSH in tumor cells derived from different human systems. According to the quantitative fluorescence intensities in Figure 2e, the respective cell lines preserved different levels of intracellular GSH. These observations were again proved by flow cytometry analyses, as indicated in Figure 2h,k. The sensitivity of the fluorescent probe in imaging intracellular GSH was further validated, using FaDu cells as the testing model. As illustrated in Figure 2c, *N*-ethylmaleimide (NEM, 5 mM), a thiol scavenger, was utilized to deplete the intracellular GSH. For the other three groups: Hcy (5 mM), glutathione monoethylester (GSH-MEE, 5 mM), and Cys (0.5 mM) were separately added in each group and incubated for 30 min. After being washed with phosphate-buffered saline (PBS, pH 7.4) for three times and then adding fresh cell culture medium, these cells were incubated with 10 μM **Cou-Br** for 10 min. Since the intracellular GSH was removed by NEM, no fluorescence signal was observed in the NEM group (Figure 2c). Compared to the Hcy and GSH-MEE group, the fluorescence in the Cys group was much stronger, which indicated that the exogenous Cys was more efficiently converted to GSH than Hcy and GSH-MEE in cells.

DOI: 10.1021/acssensors.9b02118
ACS Sens. 2020, 5, 242−249

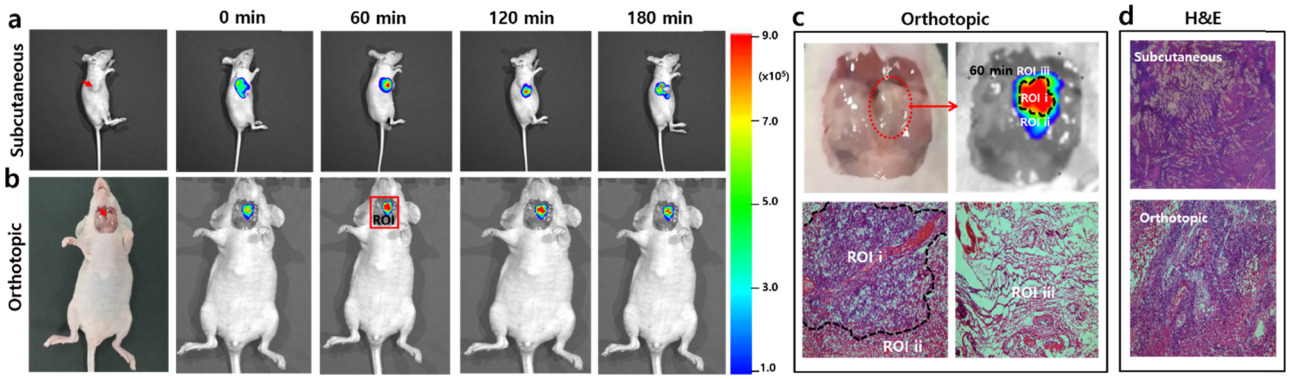

Figure 4. Time-dependent fluorescence images in subcutaneous and orthotopic laryngeal carcinoma mice models (λ_{ex} = 480 nm, λ_{em} = 500−550 nm). (a) Fluorescence images of GSH with **Cou-Br** (intertumoral injection, 50 μM, 50 μL in DMSO/saline = 1:99, v/v) in subcutaneous laryngeal cancer mice model. (b) Fluorescence images of GSH with **Cou-Br** (local spray, 50 μM, 50 μL in DMSO/saline = 1:99, v/v) in orthotopic laryngeal cancer mice model. The red arrows indicated the location of subcutaneous and orthotopic tumor, respectively. (c) Region of interest (ROI): the imaging and H&E staining of orthotopic tumor with **Cou-Br** for 60 min. (d) H&E staining of subcutaneous and orthotopic laryngeal cancer tissue, respectively.

The results obtained by flow cytometry tests (Figure 2i,l) were in well accordance with the above imaging outcomes, which further demonstrated the sensitive imaging of GSH with **Cou-Br** in biological environments.

Variation of GSH Levels under CS_2 Stimulation. Carbon disulfide (CS_2) is a commonly used organic solvent and industrial raw material. It can be easily absorbed by oral, respiratory, or skin route and distributed to the whole tissues and organs in vivo and then greatly increase the levels of ROS (e.g., H_2O_2) in living cells, which, in turn, lead to apoptosis through multiple signaling pathways.[36,37] Owing to the ROS-scavenging function of biothiols, the intracellular GSH level would be directly varied by the exogenous ROS stimulant, which could be detected by the probe **Cou-Br**. Since the developed probe had been successfully applied to detect exogenous and endogenous GSH in living cells, we were interested in investigating the probe's capability in sensing the dynamic changes of GSH by adding CS_2 stimulant to FaDu cells. In this experiment, two groups of FaDu cells were separately incubated with Cys (100 μM, 24 h) and CS_2 (5 μM, 6 h). A third group was sequentially treated with Cys (100 μM, 24 h) and CS_2 (5 μM, 6 h). As illustrated in Figure 3a, the cells treated with Cys exhibited a stronger fluorescence signal than that of the control group in Ch1. In the red channels (H_2O_2 probe CY-PFS, which was previously reported by our group[38]), the fluorescence signal of cells treated with Cys is higher than that of the control group in Ch2 but lower than that of the control group in Ch3, thus resulting in a weaker ratiometric signal (Ch3/Ch2) than that of the control group. These results suggested that the intracellular GSH levels increased, while H_2O_2 levels obviously decreased after the addition of exogenous Cys. When only incubated with CS_2, the cells offered a nearly invisible fluorescence in Ch1 but exhibited a high ratiometric signal (Ch3/Ch2) in the red channels. This phenomenon could be interpreted by the marked decrease of GSH and significant increase of H_2O_2 levels in cells upon the addition of a dose of exogenous CS_2. After supplying Cys and CS_2 in sequence to the cells, the fluorescence images were weaker than that of the Cys group, while stronger than that of the CS_2 group in Ch1. Conversely, in the red channel, this group of cells displayed a weaker ratiometric signal (Ch3/Ch2) than that of the CS_2 group but stronger than that of the Cys group (Figure 3a). These results elucidated that although the level of intracellular H_2O_2 could increase under the stimulation of CS_2, the external Cys-derived GSH could neutralize the burst of H_2O_2 in cells. Furthermore, flow cytometry analysis was performed (Figure 3e,g), outcomes of which were well consistent with the quantitative results of bioimaging (Figure 3d,f). Moreover, the cells in the CS_2 group became obviously round and were in a semiadherent state compared to those in the control group (Figure S5d). This result displayed that the addition of CS_2 could induce apoptosis. Following, the apoptosis of the four groups of cells was also measured via flow cytometry approach. As illustrated in Figure 3c, the ratio of apoptotic cells in the Cys + CS_2 group (34.41%, Q2 + Q3) was lower than that in the CS_2 group (65.18%, Q2 + Q3). The apoptosis rate of the Cys group (3.53%, Q2 + Q3) was reduced compared with that of the control group (6.91%, Q2 + Q3). These results revealed that the exogenous CS_2 could induce the burst of intracellular H_2O_2 and cause severe oxidative damage, accompanied by the decrease of GSH concentration and induced apoptosis. The addition of Cys (converted to GSH in cells) would scavenge ROS and maintain the redox homeostasis of the cells, thereby reducing the rate of apoptosis. Taken together, the proposed fluorescent probe **Cou-Br** could sensitively detect the fluctuation of intracellular GSH and could be employed to be a potential chemical tool to investigate the relationship between CS_2 and GSH in living cells.

In Situ and Real-Time Imaging of GSH in Laryngeal Carcinoma Mice Models. The ultimate utilization of fluorescent probe in clinic is to target tumor biomarkers for improved clinical treatment, such as early diagnosis, efficacy monitoring, surgical navigation, and prognosis evaluation.[39−41] Since GSH levels in tumors are evidently varied compared to surrounding disease-free tissues,[7] it may be possible to discriminate the boundary between tumor and disease-free tissues taking advantage of an appropriate fluorescent probe. Thus, the probe **Cou-Br** was next employed for imaging of GSH in mice borne with laryngeal carcinoma to verify whether the abnormal expression of GSH could be potentially used as an indicator to recognize surgery margin at cellular level. Orthotopic tumor-bearing and subcutaneous tumor-bearing laryngeal carcinoma mice models were treated with the inoculation of FaDu cells in larynx and armpit and then cultivated for the next experimental procedures after 3 weeks.

DOI: 10.1021/acssensors.9b02118
ACS Sens. 2020, 5, 242−249

The H&E staining of tumor tissue slices in Figure 4d shows the successfully planted tumor-bearing mice of subcutaneous and orthotopic laryngeal carcinomas. In the subcutaneous model, tumor was imaged after intertumoral injection with **Cou-Br** (50 μM, 50 μL in DMSO/saline = 1:99, v:v), while in the orthotopic model, the spray of probe **Cou-Br** (50 μM, 50 μL in DMSO/saline = 1:99, v:v) was applied at the opened surgical field. As illustrated in Figure 4a, the increasing fluorescence intensity from 0 to 60 min implied the accumulation of the probe in the subcutaneous solid tumor over time (180 min). Similar results were observed in the orthotopic models (Figure 4b). In the magnified image of the orthotopic tumor after 60 min (Figure 4c), the fluorescence signal in tumor lesion was distinctly stronger than that in the surrounding tissue, indicating the higher GSH level in tumor tissue. In the next step, we performed H&E staining of tumor tissues with strong (ROI i) and weak (ROI ii and ROI iii) fluorescence response, respectively. As expected, no cancer cells were observed in the tissues obtained from ROI ii and ROI ii (Figure 4c). The above results demonstrated that the probe could be utilized to discern tumor tissues from surrounding disease-free tissues. Thus, **Cou-Br** may as a potential chemical bioimaging tool for clinical surgical resection of laryngeal cancer.

Imaging of GSH in Clinical Specimens of Laryngeal Cancer Patients. To further validate the possibility of the developed probe **Cou-Br** to distinguish cancer margins in clinical samples, we then employed the probe to detect and image GSH in human laryngeal cancer specimens. Herein, we selected three different pathological types (preconfirmed by pathological biopsy) and resected intraoperative fresh slices of laryngeal carcinoma tissues and the surrounding disease-free tissues as the testing objects. Each type of slice was prepared on the same plane of the same tissue. The pathological diagnosis was directly confirmed via H&E staining. The fresh slices were first incubated with 10 μM **Cou-Br** for 30 min. After being washed three times with PBS, the samples were imaged with the probe Cou-Br under a confocal microscope. Figure 5a shows white-light images of the three patients obtained by the fiber laryngoscope in clinic, with the lesions indicated inside the dashed circles. Actually, it was still challenging to determine the surgical margin by the observation in clinic regardless of the pathological types of laryngeal cancer (Figure 5a). We next performed fluorescence imaging experiments of the lesion tissues and the surrounding disease-free tissues of the three patients, respectively (Figure 5a; ROI i, ii, and iii). As indicated in Figure 5b, fluorescence signals acquired in laryngeal carcinoma tissues of distinct pathological types were obviously stronger than the signals of disease-free tissues. Evaluated from the pathological features of different tissues of H&E staining results shown in Figure 5d, the three types of laryngeal carcinoma were clarified to be squamous epithelial dysplasia (Patient 1), well-differentiated (Patient 2), and poorly differentiated (Patient 3) squamous cell carcinoma. To explore the imaging depth of the two-photon probe, three-dimensional (3D) images of the cancer slices were performed and reconstructed from images at 1 μm step size along the z-axis. The 3D imaging results clearly verified the deep penetration of the whole tissues (100 μm) using our proposed fluorescent probe **Cou-Br** (Figure 5c). The z-axial sequential images of the ROI i slice at a depth interval of 10 μm are displayed in Figure 5e, which apparently elucidated the gradual changes and detailed cancer feature at different confocal planes. The above results demonstrated that the probe could be used not only for GSH imaging of dissimilar pathological types of human laryngeal cancer with deep penetrating ability but also for discriminating the tumor tissues against surrounding disease-free tissues according to the differentiated levels of GSH.

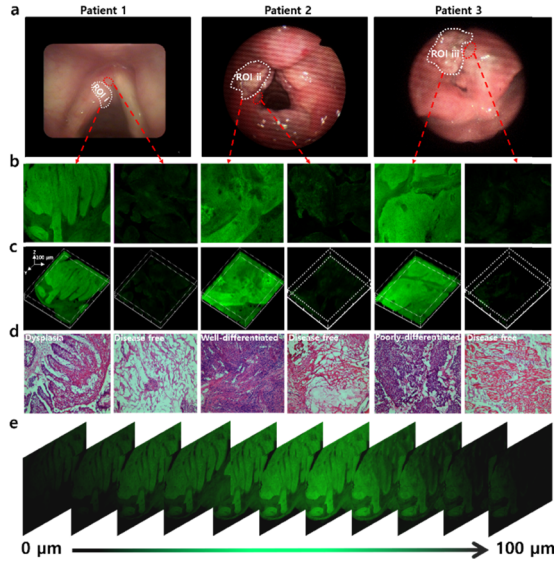

Figure 5. Fluorescence images of human fresh frozen laryngeal carcinoma of different pathological and disease-free tissue (λ_{ex} = 900 nm, λ_{em} = 500−550 nm). The slices incubated with **Cou-Br** (10 μM) for 30 min. (a) Preoperative electronic fiber laryngoscopy of the above three individual patients. (b) Fluorescence images of lesion tissues (ROI i, ii, and iii) and the surrounding disease-free tissue (100 μm thickness). (c) Three-dimensional (3D) images of (b). (d) H&E staining of (b). (e) Mapping of z-line sequential images for dysplasia slice at a depth interval of 10 μm.

CONCLUSIONS

In summary, we designed and synthesized a two-photon fluorescent probe **Cou-Br** for detecting and imaging of GSH in different living cell lines, mice models, and human cancer tissues. The probe **Cou-Br** features turn-on fluorescence, excellent two-photon imaging capability, and high selectivity and sensitivity when imaging of GSH in biological systems. The probe can sensitively detect the fluctuation of GSH in cells upon stimulation by redundant ROS. The application of the probe in tumor-bearing mice models verifies its bioimaging and tumor recognition capability in vivo. Finally, to prove the potential utilization for clinical surgery guide, the probe **Cou-Br** is successfully employed to determine the surgical margin between tumor tissue and disease-free tissue in fresh human laryngeal carcinoma specimens. Thus, the probe **Cou-Br** may provide a potential powerful chemical tool for surgical navigation of laryngeal cancer in clinic.

ASSOCIATED CONTENT

Supporting Information

The Supporting Information is available free of charge at https://pubs.acs.org/doi/10.1021/acssensors.9b02118.

Experimental materials, general methods, additional figures, synthesis steps, and compounds characterization (PDF)

DOI: 10.1021/acssensors.9b02118
ACS Sens. 2020, 5, 242−249

AUTHOR INFORMATION

Corresponding Authors

*E-mail: xingyanlong@hainmc.edu.cn (Y.X.).
*E-mail: xuejunzhou@hainmc.edu.cn (X.Z.).
*E-mail: fbyu@yic.ac.cn (F.Y.).

ORCID

Fabiao Yu: 0000-0003-0073-6299

Author Contributions

§Y.Z. and M.L. contributed equally. The manuscript was written through contributions of all of the authors. All of the authors have given approval to the final version of the manuscript.

Notes

The authors declare no competing financial interest.

ACKNOWLEDGMENTS

This work was supported by Hainan Key Research and Development Project (Grant ZDYF2019130), National Natural Science Foundation of China (Nos. 21904030 and 21775162), Hainan Higher Education Research Project (Nos. Hnky2019ZD-29 and Hnky2019ZD-30), Research Unit of Island Emergency Medicine, Chinese Academy of Medical Sciences (Grant 2019RU013), Natural Science Foundation of Hainan (No. 819MS121), Talent Program of Hainan Medical University (XRC180006 and XRC190017), and Hundred-Talent Program of Hainan (2018).

REFERENCES

(1) Kosower, N. S.; Kosower, E. M. The glutathione status of cells. *Int. Rev. Cytol.* **1978**, *54*, 109−160.

(2) Dalton, T. P.; Shertzer, H. G.; Puga, A. Regulation of gene expression by reactive oxygen. *Annu. Rev. Pharmacol. Toxicol.* **1999**, *39*, 67−101.

(3) Dröge, W.; Hack, V.; Breitkreutz, R.; Holm, E.; Shubinsky, G.; Schmid, E.; Galter, D. Role of cysteine and glutathione in signal transduction, immunopathology and cachexia. *Biofactors* **1998**, *8*, 97−102.

(4) Umezawa, K.; Yoshida, M.; Kamiya, M.; Yamasoba, T.; Urano, Y. Rational design of reversible fluorescent probes for live-cell imaging and quantification of fast glutathione dynamics. *Nat. Chem.* **2017**, *9*, 279−286.

(5) Liu, Z.; Zhou, X.; Miao, Y.; Hu, Y.; Kwon, N.; Wu, X.; Yoon, J. A Reversible Fluorescent Probe for Real-Time Quantitative Monitoring of Cellular Glutathione. *Angew. Chem., Int. Ed.* **2017**, *56*, 5812−5816.

(6) Han, X.; Song, X.; Yu, F.; Chen, L. A ratiometric fluorescent probe for imaging and quantifying anti-apoptotic effects of GSH under temperature stress. *Chem. Sci.* **2017**, *8*, 6991−7002.

(7) Gamcsik, M. P.; Kasibhatla, M. S.; Teeter, S. D.; Colvin, O. M. Gluta thione levels in human tumors. *Biomarkers* **2012**, *17*, 671−691.

(8) Bray, F.; Ferlay, J.; Soerjomataram, I.; Siegel, R. L.; Torre, L. A.; Jemal, A. Global Cancer Statistics 2018: GLOBOCAN Estimates of Incidence and Mortality Worldwide for 36 Cancers in 185 Countries. *CA Cancer J. Clin.* **2018**, *68*, 394−424.

(9) Hernot, S.; van Manen, L.; Debie, P.; Mieog, J. S. D.; Vahrmeijer, A. L. Latest developments in molecular tracers for fluorescence image-guided cancer surgery. *Lancet Oncol.* **2019**, *20*, e354−e367.

(10) Haque, R.; Contreras, R.; Mcnicoll, M. P.; Eckberg, E. C.; Petitti, D. B. Surgical margins and survival after head and neck cancer surgery. *BMC Ear, Nose Throat Disord.* **2006**, *6*, No. 2.

(11) Erickson-Bhatt, S. J.; Nolan, R. M.; Shemonski, N. D.; Adie, S. G.; Putney, J.; Darga, D.; McCormick, D. T.; Cittadine, A. J.; Zysk, A. M.; Marjanovic, M.; et al. Real-time imaging of the resection bed using a handheld probe to reduce incidence of microscopic positive margins in cancer surgery. *Cancer Res.* **2015**, *75*, 3706−3712.

(12) Vahrmeijer, A. L.; Hutteman, M.; Van Der Vorst, J. R.; Van De Velde, C. J.; Frangioni, J. V. Image-guided cancer surgery using near-infrared fluorescence. *Nat. Rev. Clin. Oncol.* **2013**, *10*, 507−518.

(13) Tanei, T.; Pradipta, A. R.; Morimoto, K.; Fujii, M.; Arata, M.; Ito, A.; Yoshida, M.; Saigitbatalova, E.; Kurbangalieva, A.; Ikeda, Ji.; et al. Cascade Reaction in Human Live Tissue Allows Clinically Applicable Diagnosis of Breast Cancer Morphology. *Adv. Sci.* **2019**, *6*, No. 1801479.

(14) Chi, C.; Du, Y.; Ye, J.; Kou, D.; Qiu, J.; Wang, J.; Tian, J.; Chen, X. Intraoperative imaging-guided cancer surgery: from current fluorescence molecular imaging methods to future multi-modality imaging technology. *Theranostics* **2014**, *4*, 1072−1084.

(15) Verdoes, M.; Edgington, L. E.; Scheeren, F. A.; Leyva, M.; Blum, G.; Weiskopf, K.; Bachmann, M. H.; Ellman, J. A.; Bogyo, M. A nonpeptidic cathepsin S activity-based probe for noninvasive optical imaging of tumor-associated macrophages. *Chem. Biol.* **2012**, *19*, 619−628.

(16) Gao, R. W.; Teraphongphom, N. T.; van den Berg, N. S.; Martin, B. A.; Oberhelman, N. J.; Divi, V.; Kaplan, M. J.; Hong, S. S.; Lu, G.; Ertsey, R.; et al. Determination of tumor margins with surgical specimen mapping using near-infrared fluorescence. *Cancer Res.* **2018**, *78*, 5144−5154.

(17) Wu, D.; Sedgwick, A. C.; Gunnlaugsson, T.; Akkaya, E. U.; Yoon, J.; James, T. D. Fluorescent chemosensors: the past, present and future. *Chem. Soc. Rev.* **2017**, *46*, 7105−7123.

(18) Meng, W.; Sun, M.; Xu, Q.; Cen, J.; Cao, Y.; Li, Z.; Xiao, K. Development of a series of fluorescent probes for the early diagnostic imaging of sulfur mustard poisoning. *ACS Sens.* **2019**, *4*, 2794−2801.

(19) Kolanowski, J. L.; Liu, F.; New, E. J. Fluorescent probes for the simultaneous detection of multiple analytes in biology. *Chem. Soc. Rev.* **2018**, *47*, 195−208.

(20) Tang, Y.; Lee, D.; Wang, J.; Li, G.; Yu, J.; Lin, W.; Yoon, J. Development of fluorescent probes based on protection−deprotection of the key functional groups for biological imaging. *Chem. Soc. Rev.* **2015**, *44*, 5003−5015.

(21) Cao, C.; Wei, P.; Li, R.; Zhong, Y.; Li, X.; Xue, F.; Shi, Y.; Yi, T. Ribosomal RNA-Selective Light-Up Fluorescent Probe for Rapidly Imaging the Nucleolus in Live Cells. *ACS Sens.* **2019**, *4*, 1409−1416.

(22) Li, H.; Li, X.; Shi, W.; Xu, Y.; Ma, H. Rationally Designed Fluorescence ·OH Probe with High Sensitivity and Selectivity for Monitoring the Generation of ·OH in Iron Autoxidation without Addition of H2O2. *Angew. Chem., Int. Ed.* **2018**, *130*, 13012−13016.

(23) He, L.; Xu, Q.; Liu, Y.; Wei, H.; Tang, Y.; Lin, W. Coumarin-based turn-on fluorescence probe for specific detection of glutathione over cysteine and homocysteine. *ACS Appl. Mater. Interfaces* **2015**, *7*, 12809−12813.

(24) Yin, J.; Kwon, Y.; Kim, D.; Lee, D.; Kim, G.; Hu, Y.; Ryu, J.; Yoon, J. Cyanine-Based Fluorescent Probe for Highly Selective Detection of Glutathione in Cell Cultures and Live Mouse Tissues. *J. Am. Chem. Soc.* **2014**, *136*, 5351−5358.

(25) Yu, F.; Li, P.; Wang, B.; Han, K. Reversible near-infrared fluorescent probe introducing tellurium to mimetic glutathione peroxidase for monitoring the redox cycles between peroxynitrite and glutathione in vivo. *J. Am. Chem. Soc.* **2013**, *135*, 7674−7680.

(26) Lee, S.; Li, J.; Zhou, X.; Yin, J.; Yooh, J. Recent Progress on the Development of Glutathione (GSH) Selective Fluorescent and Colorimetric Probes. *Coord. Chem. Rev.* **2018**, *366*, 29−68.

(27) Kim, H. J.; Heo, C. H.; Kim, H. M. Benzimidazole-based ratiometric two-photon fluorescent probes for acidic pH in live cells and tissues. *J. Am. Chem. Soc.* **2013**, *135*, 17969−17977.

(28) Li, S.-J.; Zhou, D.-Y.; Li, Y.; Liu, H.-W.; Wu, P.; Ou-Yang, J.; Jiang, W.-L.; Li, C.-Y. Efficient two-photon fluorescent probe for imaging of nitric oxide during endoplasmic reticulum stress. *ACS Sens.* **2018**, *3*, 2311−2319.

(29) Tang, Y.; Kong, X.; Xu, A.; Dong, B.; Lin, W. Development of a Two-Photon Fluorescent Probe for Imaging of Endogenous Formaldehyde in Living Tissues. *Angew. Chem., Int. Ed.* **2016**, *55*, 3356−3359.

DOI: 10.1021/acssensors.9b02118
ACS Sens. 2020, 5, 242−249

(30) Sun, W.; Fan, J.; Hu, C.; Cao, J.; Zhang, H.; Xiong, X.; Wang, J.; Cui, S.; Sun, S.; Peng, X. A two-photon fluorescent probe with near-infrared emission for hydrogen sulfide imaging in biosystems. *Chem. Commun.* **2013**, *49*, 3890−3892.
(31) Riveiro, M. E.; Kimpe, N. De.; Moglioni, A.; Vazquez, R.; Monczor, F.; Shayo, C.; Davio, C. Coumarins: Old compounds with novel promising therapeutic perspectives. *Curr. Med. Chem.* **2010**, *17*, 1325−1338.
(32) Cao, D.; Liu, Z.; Verwilst, P.; Koo, S.; Jangjili, P.; Kim, J. S.; Lin, W. Coumarin-Based Small-Molecule Fluorescent Chemosensors. *Chem. Rev.* **2019**, *119*, 10403−10519.
(33) Rossi, R.; Giustarini, D.; Milzani, A.; Dalle-Donne, I. Cysteinylation and homocysteinylation of plasma protein thiols during ageing of healthy human beings. *J. Cell. Mol. Med.* **2009**, *13*, 3131−3140.
(34) Lakowicz, J. R. *Principles of Fluorescence Spectroscopy*; Springer Science & Business Media, 2013.
(35) Xu, C.; Webb, W. W. Measurement of two-photon excitation cross sections of molecular fluorophores with data from 690 to 1050 nm. *J. Opt. Soc. Am. B* **1996**, *13*, 481−491.
(36) DeMartino, A. W.; Zigler, D. F.; Fukuto, J. M.; Ford, P. C. Carbon disulfide. Just toxic or also bioregulatory and/or therapeutic? *Chem. Soc. Rev.* **2017**, *46*, 21−39.
(37) Domergue, J.; Lison, D.; Haufroid, V. No evidence of cardiovascular toxicity in workers exposed below 5 ppm carbon disulfide. *Int. Arch. Occup. Environ. Health* **2016**, *89*, 835−845.
(38) Guo, H.; Chen, G.; Gao, M.; Wang, R.; Liu, Y.; Yu, F. Imaging of endogenous hydrogen peroxide during the process of cell mitosis and mouse brain development with a near-infrared ratiometric fluorescent probe. *Anal. Chem.* **2019**, *91*, 1203−1210.
(39) Liu, H.; Chen, L.; Xu, C.; Li, Z.; Zhang, H.; Zhang, X.; Tan, W. Recent progresses in small-molecule enzymatic fluorescent probes for cancer imaging. *Chem. Soc. Rev.* **2018**, *47*, 7140−7180.
(40) Gao, M.; Yu, F.; Lv, C.; Choo, J.; Chen, L. Fluorescent chemical probes for accurate tumor diagnosis and targeting therapy. *Chem. Soc. Rev.* **2017**, *46*, 2237−2271.
(41) Zhang, J.; Chai, X.; He, X.; Kim, H.; Yoon, J.; Tian, H. Fluorogenic probes for disease-relevant enzymes. *Chem. Soc. Rev.* **2019**, *48*, 683−722.

DOI: 10.1021/acssensors.9b02118
ACS Sens. 2020, 5, 242−249